Int J Adv Manuf Technol (2017) 90:1679–1691
DOI 10.1007/s00170-016-9507-2

ORIGINAL ARTICLE

Hybrid analytic-experimental modeling for machine tool structural dynamics

Bosheng Ye[1] · **Weiwei Xiao**[2] · **Kuanmin Mao**[1] · **Bin Li**[1]

Received: 26 May 2016 / Accepted: 16 September 2016 / Published online: 29 September 2016

Abstract The usage of virtual prototype technology to study the static and dynamic properties of machine tools could shorten the life cycle time of machine design as there is no need for a physical prototype. The base of this technology is to establish the virtual model accurately and conveniently. This study presents a hybrid analytic-experimental method for the dynamic modeling of machine tools. In the proposed method, the structural components of machine tools are modeled by an analytic method (finite element method), and the machine elements are represented by models that originate from experimental data. The full dynamic model of the machine tool structure is obtained by assembling the analytic models of the structural components and experimental models of the machine elements. The bolted joint is taken as an example to illustrate the experimental model for the machine elements and the assembly of the analytic and experimental models. The convenience and accuracy of the proposed hybrid analytic-experimental modeling method are illustrated by two engineering examples.

Keywords Hybrid analytic-experimental modeling · Machine tool · Structural dynamics · Bolted joint

✉ Kuanmin Mao
kmmao4645@sina.com.cn

[1] National NC System Engineering Research Center, Huazhong University of Science and Technology, Wuhan 430074, People's Republic of China

[2] School of Mechanical Science and Engineering, Huazhong University of Science and Technology, Wuhan 430074, People's Republic of China

1 Introduction

Machine tools are very complex electromechanical systems. Currently, with the rapid development in the aircraft, automobile, aerospace, marine, and equipment manufacturing industries, machine tools with high precision and a high cutting speed are in urgent need, and the design cycle is becoming progressively tighter. Thus, the traditional mode of production for machine tools (for example the cycle of design, manufacture, experiment, and adjustment) cannot meet such requirements. Fortunately, the development of computer simulation technology and virtual machine tools provides a possible solution to this problem. The virtual machine tool is a simulation of the entire machine tool. It involves the structure of the machine tool and a computer numerical control system. Research into the virtual machine tool has attracted more and more attention at research institutes [1–7]. Using the virtual machine tool model, one can obtain the kinematics and structural dynamics, which notably influence the performance of the machine tools.

To meet all the requirements of the virtual machine tool in the best possible way, an accurate physical prototype must be established first. In the past decades, many studies have been performed on the issue. These studies are generally based on one of the following three models: finite element method (FEM) [8–15], multibody simulation [16–18], and discrete mass-spring-damper models [19–21]. In addition, Zaeh and Seidl [22] presented a method for modeling machine tools by integrating the finite element method with multibody simulations. The same method was also employed by Brecher and Witt [4]. Because of the complexity of the machine tool's structure, a hybrid theoretical-experimental modeling method has been proposed in previous studies [23, 24].

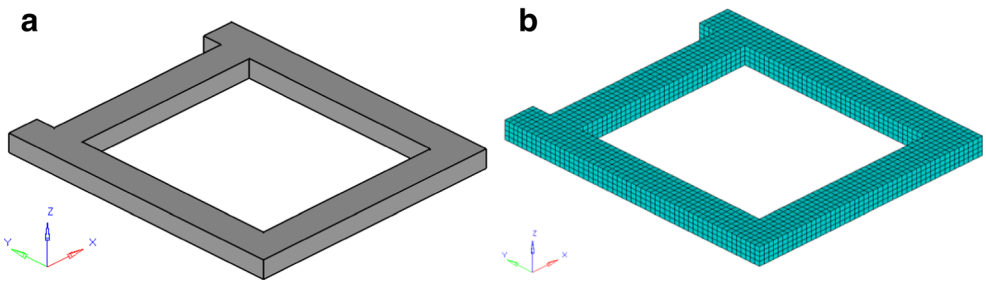

Fig. 1 Component models: **a** geometry model and **b** FE model using hexahedral elements

According to one of the proposed methods, the static and dynamic performance of a machine tool can be estimated. However, as shown in reference [13], the comparison between simulated and the measured data revealed that the flexibility of the machine element connections cannot be neglected. Thus, the modeling of connections in the machine tool must be taken into consideration when modeling an entire machine tool structure.

Generally speaking, a whole machine tool structure is composed of many components connected by joints. Studies have documented that more than 60 % of dynamic stiffness originates from the joints [25], and as much as 90 % of damping of an entire machine tool structure is contributed by the joints [26]. The characteristics of the joints notably affect the performance of the entire machine tool structure. Thus, an accurate model of the joints must be formulated to model the entire machine tool structure. Studies on modeling joints in machine tools, such as the bolted [27–29], spindle-holder taper [30–33], ball screw [34, 35], and guideway joint [36–38], have attracted considerable interest in the research community. However, due to their complexity, there is no universal model for these joints. In many cases, the proposed model is suitable only for the specific condition. Thus, the modeling method of joints in machine tools is still a desirable research focus.

In a previous study [29], based on the stiffness influential coefficient method, a dynamic model of the bolted joint in machine tools was proposed. Based on the dynamic model, the relationship between the stiffness of the bolted joint element and the three influential factors (preload, geometric dimension, and contact surface roughness) was deduced, and a parameterized model of the bolted joint was established [39]. In this study, taking the modeling of a bolted joint as an example, we propose a hybrid analytic-experimental modeling method for machine tool structural dynamics, and two applications are shown to illustrate the proposed modeling method, which provides a possible way to obtain a full dynamic model of a machine tool.

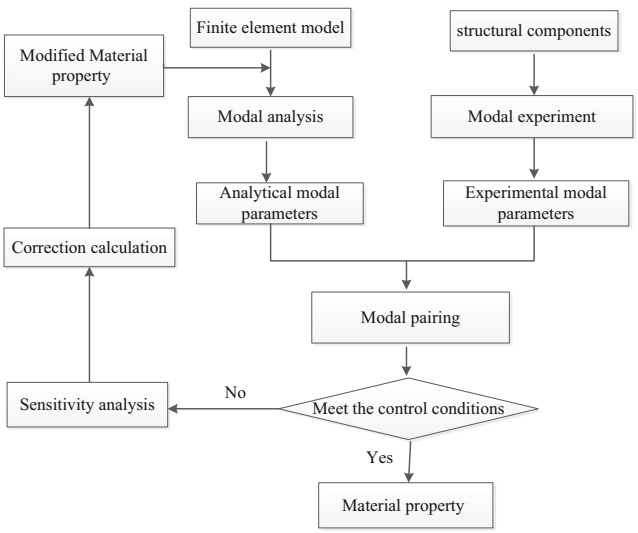

Fig. 2 The progress in the determination of material properties

2 Dynamic modeling method of the machine tool structures

According to the illustrations in the literature [4], machine tool structures are divided into structural components and machine elements. Structural components refer to the main frame structures of the machine, such as bed, column, base, and spindle housing. Machine elements are the connection between structural components, such as the bolted joint, guiding systems, bearings, and ball screw drives. The dynamic modeling method of structural components and machine elements is conceptualized in the following sections.

2.1 Modeling structural components of the machine tool

The dynamic model of the structural components is established using the FEM. Finite element (FE) software, such as MSC.patran, Ansys, and Abaqus, provides the finite elements to establish the dynamic model. However, the material parameters will influence the accuracy of the FE model.

Table 1 The determined material parameters

E (GPa)	μ	ρ (kg/m^3)
121	0.27	7340

Table 2 The experimental and numerical results

Mode shape	Natural frequencies (Hz)		
	Modal test results	FE model analysis	Error (%)
Y-axis first-order reversing	123.5	125.7	−1.78
X-axis first-order bending	212.4	218.3	−2.77
Z-axis first-order reversing	248.7	236.5	4.90
Y-axis first-order bending	363.6	377.7	−3.87
X-axis first-order reverse bending	380.1	383.8	−0.97
Y-axis first-order reverse bending	435.7	449.1	−3.07

In general, the structural components of machine tools are constituted by cast iron using a casting molding method. It is well known that the material parameters of cast iron, such as elastic modulus and mass density, have not been determined. Thus, it is necessary to determine accurate material parameters when modeling a component made of cast iron. The mass density can be obtained by dividing the mass by the volume. However, the elastic modulus is not acquired as easily. In this study, a method based on the modal test is used to determine the elastic modulus of the component, which is shown in Fig. 1.

The progress toward parameter determination is shown in Fig. 2. First, the experimental modal parameters of the component, such as natural frequencies and corresponding mode shapes, are obtained when modal testing is executed with free-to-free boundary conditions. Then, the FE model of this component is established using hexahedral elements, as shown in Fig. 1b. The elastic modulus values are in the range of 78.5 to 157 GPa, and Poisson's ratio ranges from 0.23 to 0.29. After a normal mode analysis, the simulated modal parameters can be obtained. To minimize the error associated with experimental and simulated natural frequencies, an accurate elastic modulus is obtained, which is shown in Table 1. As shown in Table 2, the largest error in the natural frequency under the same mode shape in both modal test results and the FE model analysis is less than 5 %, which illustrated the accuracy of material parameters.

2.2 Modeling machine elements of the machine tool

The characteristics of the machine elements notably influence the performance of the machine tool, as mentioned above. Because of the complexity, modeling machine elements is a difficult task. In this study, dynamic modeling of a bolted joint is taken as an example to illustrate the modeling of machine elements of a machine tool.

2.2.1 General forms of bolted joint in machine tool structure

After analyzing the form of the bolted joint in many types of machine tools, such as the MC6000 Plano machining center driven by a linear motor, CKX5680 seven-five axis lathe-milling CNC equipment, XHK5140 CNC machine tool, and EQD18A-40 high-speed machining center, the general forms of the bolted joint are extracted, as listed in Fig. 3.

2.2.2 Dynamic modeling of the bolted joint

The joint structures in Fig. 3a, c are in the form of a "linear" connection, while in Fig. 3b, it is in the form of an "array" connection. Inspired by the St. Venant assumption, we make the following assumptions about the dynamic characteristics of the bolted joint.

For the "linear" connection form, it is assumed that the dynamic characteristics of the joints between two adjacent bolts are only affected by the mechanical attributes of the

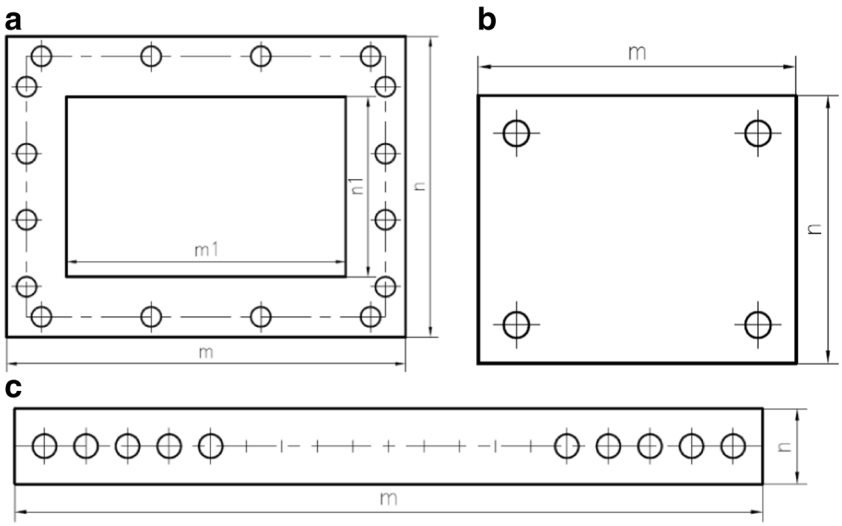

Fig. 3 General form of the bolted joint in machine tools: **a** beam-column connection, **b** slide block-slider connection, and **c** beam-rail connection

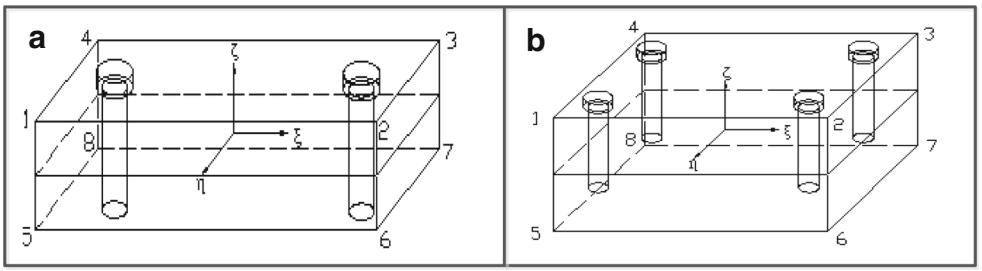

Fig. 4 Bolted joint elements: **a** "linear" connection and **b** "array" connection

two adjacent bolts and have nothing to do with the other bolts, and for the "array" connection, the dynamic characteristics of the joints between four adjacent bolts are only affected by the mechanical attributes of the four adjacent bolts and have nothing to do with the other bolts. The assumptions made above have been proven in a previous study [29].

According to the above assumptions, the joint between each two adjacent bolts is regarded as a bolted joint element in the 'linear' connection form, as shown in Fig. 4a. For the "array" connection, the joint between each four adjacent bolts is regarded as a bolted joint element, as shown in Fig. 4b. Each element has 8 nodes, and every node has 3 translational degrees of freedom (DOFs), so every bolted joint element has 24 DOFs. The movements of the joints are represented by relative movements between nodes 1 and 5, 2 and 6, 3 and 7, and 4 and 8. Once the exact relation between the forces on these nodes and their displacements is determined, the dynamic model of the bolted joint is established.

n this study, only the elasticity and damping characteristics of the bolted joint are taken into consideration, regardless of the mass. Suppose that the node displacement is x_{ij}, and the node force is f_{ij} ($i = 1, 2, \ldots, 7, 8; j = 1, 2, 3$). First of all, the stiffness matrix of the bolted joint elements is deduced. As mentioned above, the movements of joints are represented in the form of relative movements between node pairs, and the relative movements between these nodes are expressed as

$x_{1j}-x_{5j}, x_{2j}-x_{6j}, x_{3j}-x_{7j}, x_{4j}-x_{8j}$ where $j = 1, 2, 3$.

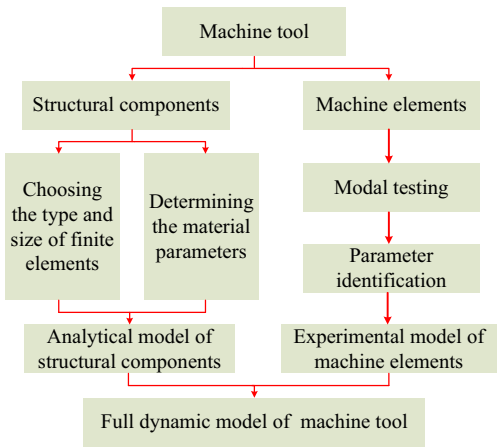

Fig. 5 Hybrid analytic-experimental modeling method of machine tools

According to the stiffness influential coefficient method, there is

$$\sum_{n=1}^{3} K_{1n}^{ij}(x_{1n}-x_{5n}) + \sum_{n=1}^{3} K_{2n}^{ij}(x_{2n}-x_{6n}) + \sum_{n=1}^{3} K_{3n}^{ij}(x_{3n}-x_{7n}) + \sum_{n=1}^{3} K_{4n}^{ij}(x_{4n}-x_{8n}) = f_{ij} \quad (1)$$

where K_{1n}^{ij} is the stiffness influential coefficient; i, $m = 1$, 2, 3, 4 is the number of nodes; and n, $j = 1$, 2, 3 represents the direction. K_{1n}^{ij} is the corresponding necessary force applied to node i in the j direction when the unit relative displacement is only generated between node m and node $m+4$ in the n direction. Thus, under equilibrium conditions, the relationship of the node force can be expressed as

$$f_{1j} = -f_{5j}; f_{2j} = -f_{6j}; f_{3j} = -f_{7j}; f_{4j} = -f_{8j} \quad (2)$$

with $\{\mathbf{x}\} = (x_{11}, x_{12}, x_{13}, \ldots, x_{81}, x_{82}, x_{83})$ and $\{\mathbf{f}\} = (f_{11}, f_{12}, -f13, \ldots, f_{81}, f_{82}, f_{83})$, Eq. (1) can be written as

$$[\mathbf{K}]\{\mathbf{x}\} = \{\mathbf{f}\} \quad (3)$$

where $[\mathbf{K}]$ is a 24×24 symmetric matrix, and $[\mathbf{K}] = [K' \quad -K' \quad -K' K']$.

From the force and displacement hysteresis loop, the structural damping coefficient, η, of the finite element model can be derived. Thus, the dynamic equation of the bolted joint element can be obtained as follows:

$$(i\eta[\mathbf{K}] + [\mathbf{K}])\{\mathbf{x}\} = \{\mathbf{f}\} \quad (4)$$

2.2.3 Identification of parameters of the bolted joint

The dynamic equation of a multidegree-of-freedom linear vibration system that contains joints can be expressed as (in frequency domain)

$$\left([\mathbf{K}_s] + j\eta[\mathbf{K}_e] + [\mathbf{K}_e] + j\omega[\mathbf{C}_s] - \omega^2[\mathbf{M}_s]\right)\{\mathbf{X}(\omega)\} = \{\mathbf{F}(\omega)\} \quad (5)$$

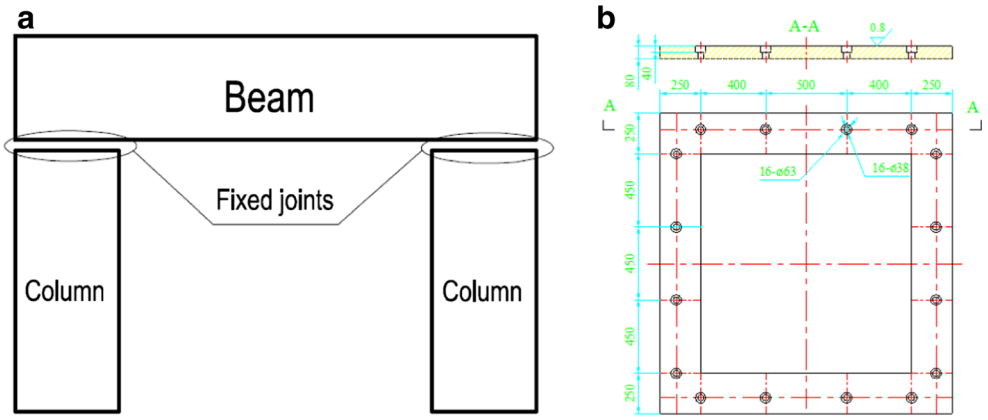

Fig. 6 Connection model of the beam and column: **a** a schematic drawing of the connection and **b** plane dimension of the bolted joint

where $[\mathbf{K}_s]$, $[\mathbf{C}_s]$, and $[\mathbf{M}_s]$ are the stiffness matrix, damping matrix, and mass matrix of the machine tools' structural components; $[\mathbf{K}_e]$ is the stiffness matrix of the bolted joint element, and η is the damping coefficient. The dynamic stiffness matrix of the system can be expressed as

$$[\mathbf{Z}(\omega)] = [\mathbf{K}_s] + j\eta[\mathbf{K}_e] + [\mathbf{K}_e] + j\omega[\mathbf{C}_s] - \omega^2[\mathbf{M}_s] \tag{6}$$

According to the definition of frequency response function (FRF),

$$\{\mathbf{H}(\omega)\}\{\mathbf{F}(\omega)\} = \{\mathbf{X}(\omega)\} \tag{7}$$

Thus, we can obtain the following equation:

$$\{\mathbf{Z}(\omega)\}\{\mathbf{H}(\omega)\} = \mathbf{I} \tag{8}$$

When a hammer impact testing is implemented on an N-DOF system in a manner of single input and multiple output (SIMO), the driving point is fixed at coordinate j; the response point is moved to a different coordinate i ($i = 1, 2, \ldots, N$), and the jth column of the FRF matrix can be obtained. Based on Eqs. (6) and (8), there is

$$([\mathbf{K}_s] + j\eta[\mathbf{K}_e] + [\mathbf{K}_e] + j\omega[\mathbf{C}_s] - \omega^2[\mathbf{M}_s]) \begin{Bmatrix} \mathbf{H}_{1j}(\omega) \\ \vdots \\ \mathbf{H}_{i-1j}(\omega) \\ \mathbf{H}_{ij}(\omega) \\ \mathbf{H}_{i+1j}(\omega) \\ \vdots \\ \mathbf{H}_{nj}(\omega) \end{Bmatrix} = \begin{Bmatrix} 0 \\ \vdots \\ 0 \\ 1 \\ 0 \\ \vdots \\ 0 \end{Bmatrix} \tag{9}$$

The matrices $[\mathbf{K}_s]$, $[\mathbf{C}_s]$, and $[\mathbf{M}_s]$ in Eq. (9) can be obtained by FEMs. Thus, according to Eq. (9), the unknown parameters $[\mathbf{K}_e]$ and η of the linear vibration system can be identified using the nonlinear least square method.

2.2.4 Bolted joint element stiffness matrix database

In a previous study [39], we summarized the influential factors of bolted joint dynamic characteristics as preload (mainly caused by the pretightened torque of bolt),

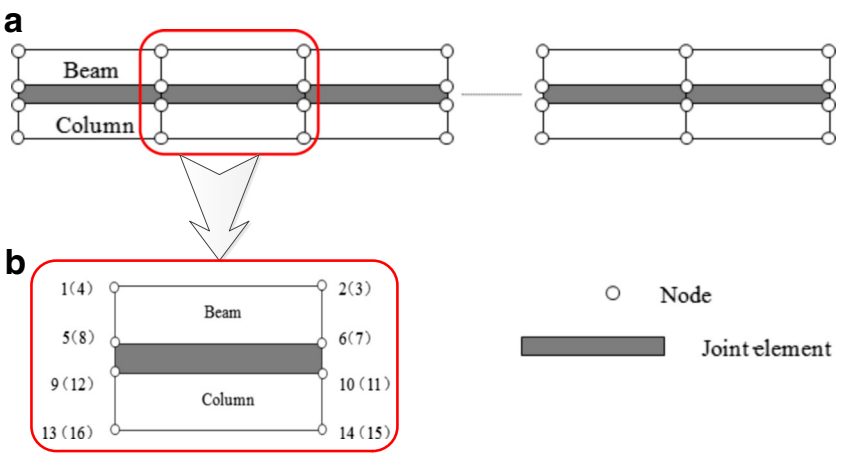

Fig. 7 FE model of the beam-column assembly connected by joint elements: **a** all connections and **b** one connection

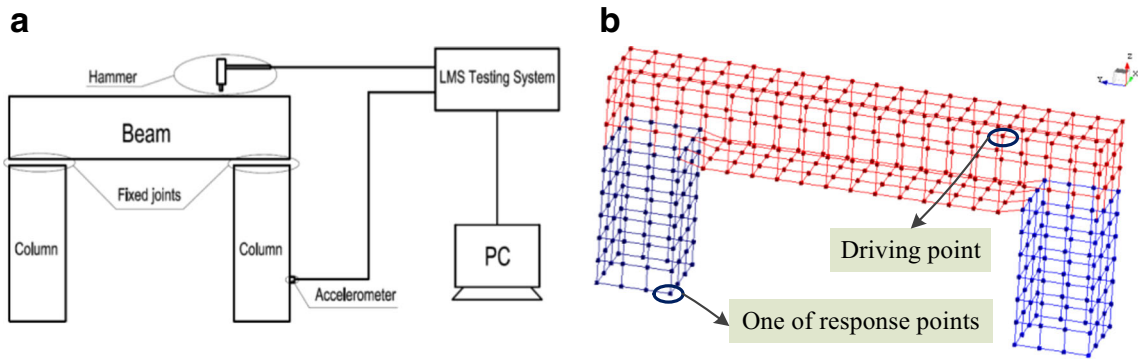

Fig. 8 Experimental system: **a** the testing setup and **b** a schematic drawing of the driving point and response points

geometric dimension, and contact surface roughness. We deduced the relationship between the stiffness of the bolted joint element and the three influential factors. Based on this relationship, the bolted joint element stiffness matrix database is established. Thus, if the preload, geometric dimension, and contact surface roughness are determined, the stiffness matrix of the bolted joint element can be obtained.

3 Hybrid analytic-experiment modeling method of machine tool

As discussed in the above section, the dynamic model of the structural components can be established by the FEM, and the dynamic model of the machine elements can be established by the proposed experiment-based dynamic model. Assembling the two models accurately is a problem that must be addressed in the dynamic modeling of the entire machine tool. In this section, a hybrid analytic-experimental modeling method of the machine tool is illustrated, which is shown in Fig. 5.

In this study, the bolted joint between the beam and column of a seven-five axis machine tool, which is shown in Fig. 6, is used as an example to show the proposed analytic-experimental modeling method. The beam and two columns are connected by 16 M36 bolts, and the distribution of the bolts is shown in Fig. 6b. By the analytic-experimental modeling method proposed in this paper, the column (analytic FE model), joints (experimental FE model), and beam (analytic FE model) are assembled into the dynamic FE model, which is shown in Fig. 7.

For every joint element in the dynamic model shown in Fig. 7, the stiffness matrix, $[\mathbf{K}_e]$, and the damping coefficient, η, are acquired by the proposed parameter identification method. The dynamic equation of the joint element is expressed as Eq. (3). According to the FEM theory, the FE model is connected as a whole structure by many nodes, and the forces are transferred by these nodes. The assembly of the dynamic

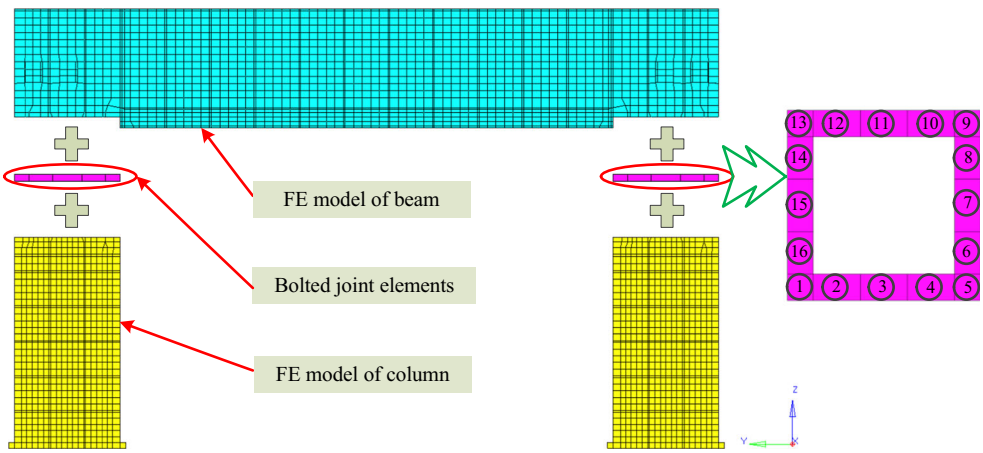

Fig. 9 FE model of the seven-five axis machine tool

Table 3 Material parameters of the components

E (GPa)	μ	ρ (kg/m^3)
120	0.27	7500

equations of one connection is composed of two finite elements of the structural components and a joint element, as illustrated in Fig. 6b.

The dynamic equation of the beam element (the element number is 1) can be written as

$$[\mathbf{K}^1]\begin{Bmatrix}\mathbf{x}_{1,1}\\ \mathbf{x}_{2,1}\\ \vdots\\ \mathbf{x}_{8,2}\\ \mathbf{x}_{8,3}\end{Bmatrix}=\begin{bmatrix}\mathbf{K}_a^1 & \mathbf{K}_b^1\\ \mathbf{K}_c^1 & \mathbf{K}_d^1\end{bmatrix}\begin{Bmatrix}\mathbf{x}_{1,1}\\ \mathbf{x}_{2,1}\\ \vdots\\ \mathbf{x}_{8,2}\\ \mathbf{x}_{8,3}\end{Bmatrix}=\begin{Bmatrix}f_{1,1}^1\\ f_{1,2}^1\\ \vdots\\ f_{8,2}^1\\ f_{8,3}^1\end{Bmatrix} \tag{10}$$

Table 4 Experimental and FEM simulation modal shapes

Modal	Experimental modal shapes	FEM simulation modal shapes	MAC
1	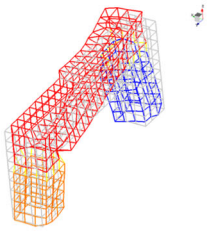	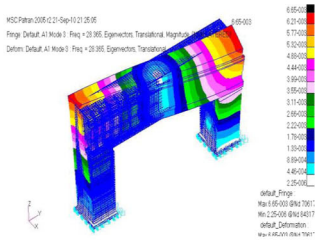	0.904
2	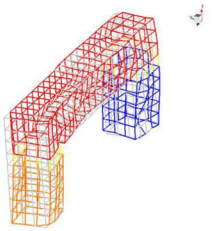	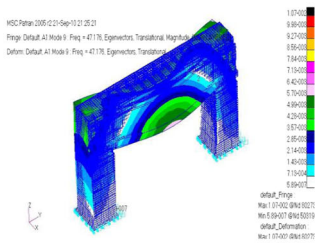	0.945
3	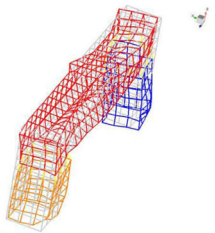	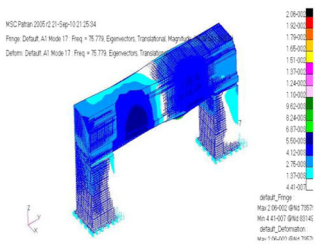	0.936
4	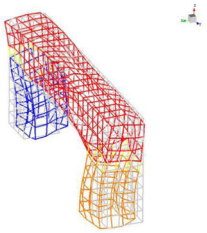	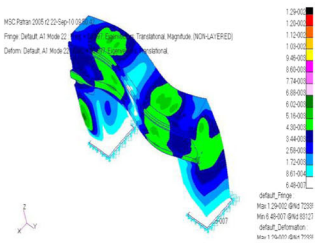	0.958
5	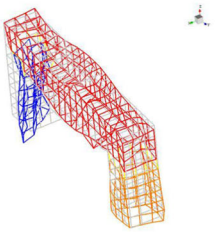	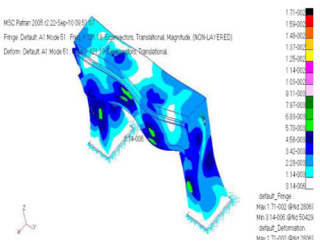	0.929

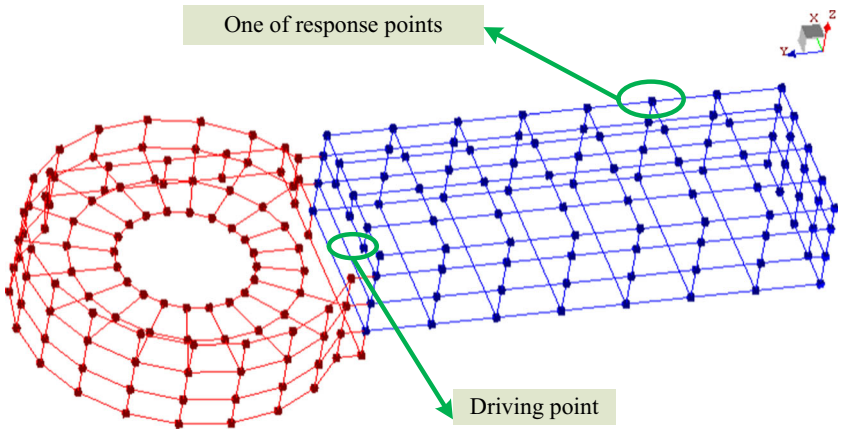

Fig. 10 The schematic drawing of the driving point and response points

where

$$\mathbf{K}_{\mathrm{a}}^{1}=\begin{bmatrix} k_{1,1}^{1} & \cdots & k_{1,12}^{1} \\ \vdots & \ddots & \vdots \\ k_{12,1}^{1} & \cdots & k_{12,12}^{1} \end{bmatrix};\mathbf{K}_{\mathrm{b}}^{1}$$

$$=\begin{bmatrix} k_{1,13}^{1} & \cdots & k_{1,24}^{1} \\ \vdots & \ddots & \vdots \\ k_{12,13}^{1} & \cdots & k_{12,24}^{1} \end{bmatrix};\mathbf{K}_{\mathrm{c}}^{1}$$

$$=\begin{bmatrix} k_{13,1}^{1} & \cdots & k_{13,12}^{1} \\ \vdots & \ddots & \vdots \\ k_{24,1}^{1} & \cdots & k_{24,12}^{1} \end{bmatrix};\mathbf{K}_{\mathrm{d}}^{1}=\begin{bmatrix} k_{13,13}^{1} & \cdots & k_{13,24}^{1} \\ \vdots & \ddots & \vdots \\ k_{24,13}^{1} & \cdots & k_{24,24}^{1} \end{bmatrix}$$

The dynamic equation of the column element (the element number is 2) can be written as

$$[\mathbf{K}^{2}]\begin{Bmatrix} \mathbf{x}_{9,1} \\ \mathbf{x}_{9,1} \\ \vdots \\ \mathbf{x}_{16,2} \\ \mathbf{x}_{16,3} \end{Bmatrix}=\begin{bmatrix} \mathbf{K}_{\mathrm{a}}^{2} & \mathbf{K}_{\mathrm{b}}^{2} \\ \mathbf{K}_{\mathrm{c}}^{2} & \mathbf{K}_{\mathrm{d}}^{2} \end{bmatrix}\begin{Bmatrix} \mathbf{x}_{9,1} \\ \mathbf{x}_{9,1} \\ \vdots \\ \mathbf{x}_{16,2} \\ \mathbf{x}_{16,3} \end{Bmatrix}=\begin{Bmatrix} f_{9,1} \\ f_{9,1} \\ \vdots \\ f_{16,2} \\ f_{16,3} \end{Bmatrix} \quad (11)$$

Table 5 Modal results comparison

Modal shape	Experimental result (Hz)	FE result (Hz)	Errors (%)
Z-axis first-order reversing	23.8	28.4	19.3
Z-axis first-order bending	44.8	47.2	5.4
Z-axis second-order bending	72.4	75.8	4.7
X-axis second-order bending	81.4	80.1	1.6
Respiratory expansion of column	122.4	121.2	0.8

where

$$\mathbf{K}_{\mathrm{a}}^{2}=\begin{bmatrix} k_{1,1}^{2} & \cdots & k_{1,12}^{2} \\ \vdots & \ddots & \vdots \\ k_{12,1}^{2} & \cdots & k_{12,12}^{2} \end{bmatrix};\mathbf{K}_{\mathrm{b}}^{2}$$

$$=\begin{bmatrix} k_{1,13}^{2} & \cdots & k_{1,24}^{2} \\ \vdots & \ddots & \vdots \\ k_{12,13}^{2} & \cdots & k_{12,24}^{2} \end{bmatrix};\mathbf{K}_{\mathrm{c}}^{2}$$

$$=\begin{bmatrix} k_{13,1}^{2} & \cdots & k_{13,12}^{2} \\ \vdots & \ddots & \vdots \\ k_{24,1}^{2} & \cdots & k_{24,12}^{2} \end{bmatrix};\mathbf{K}_{\mathrm{d}}^{2}=\begin{bmatrix} k_{13,13}^{2} & \cdots & k_{13,24}^{2} \\ \vdots & \ddots & \vdots \\ k_{24,13}^{2} & \cdots & k_{24,24}^{2} \end{bmatrix}$$

Finally, the dynamic equation of the joint element (the element number is 3) can be written as

$$[\mathbf{K}^{3}]\begin{Bmatrix} \mathbf{x}_{5,1} \\ \mathbf{x}_{5,1} \\ \vdots \\ \mathbf{x}_{12,2} \\ \mathbf{x}_{12,3} \end{Bmatrix}=[\mathbf{K}_{e}]\begin{Bmatrix} \mathbf{x}_{5,1} \\ \mathbf{x}_{5,1} \\ \vdots \\ \mathbf{x}_{12,2} \\ \mathbf{x}_{12,3} \end{Bmatrix}=\begin{bmatrix} \mathbf{K}_{\mathrm{a}}^{3} & \mathbf{K}_{\mathrm{b}}^{3} \\ \mathbf{K}_{\mathrm{c}}^{3} & \mathbf{K}_{\mathrm{d}}^{3} \end{bmatrix}\begin{Bmatrix} \mathbf{x}_{5,1} \\ \mathbf{x}_{5,1} \\ \vdots \\ \mathbf{x}_{12,2} \\ \mathbf{x}_{12,3} \end{Bmatrix}=\begin{Bmatrix} f_{5,1} \\ f_{5,1} \\ \vdots \\ f_{12,2} \\ f_{12,3} \end{Bmatrix} \quad (12)$$

where

$$\mathbf{K}_{\mathrm{a}}^{3}=\begin{bmatrix} k_{1,1}^{3} & \cdots & k_{1,12}^{3} \\ \vdots & \ddots & \vdots \\ k_{12,1}^{3} & \cdots & k_{12,12}^{3} \end{bmatrix};\mathbf{K}_{\mathrm{b}}^{3}$$

$$=\begin{bmatrix} k_{1,13}^{3} & \cdots & k_{1,24}^{3} \\ \vdots & \ddots & \vdots \\ k_{12,13}^{3} & \cdots & k_{12,24}^{3} \end{bmatrix};\mathbf{K}_{\mathrm{c}}^{3}$$

$$=\begin{bmatrix} k_{13,1}^{3} & \cdots & k_{13,12}^{3} \\ \vdots & \ddots & \vdots \\ k_{24,1}^{3} & \cdots & k_{24,12}^{3} \end{bmatrix};\mathbf{K}_{\mathrm{d}}^{3}=\begin{bmatrix} k_{13,13}^{3} & \cdots & k_{13,24}^{3} \\ \vdots & \ddots & \vdots \\ k_{24,13}^{3} & \cdots & k_{24,24}^{3} \end{bmatrix}$$

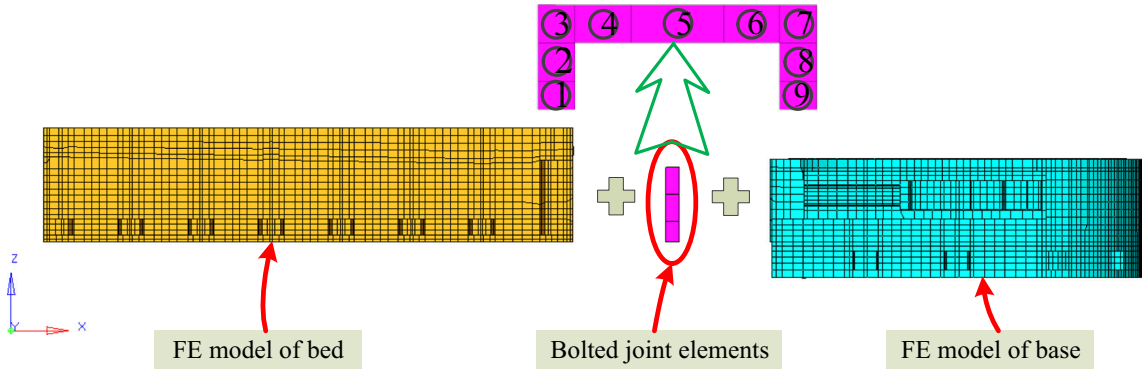

Fig. 11 FE model of the bed and base assembly

The three elements are connected by nodes 5 through 12. Here, node 5 is used as an example to illustrate how to establish the force balance equation. Node 5 is a connected node of element 1 and element 3. In the dynamic equations of element 1, the equations that are relevant to the force acting on node 5 can be written as

$$\begin{cases} k^1_{13,1}x_{1,1} + k^1_{13,2}x_{1,2} + \cdots + k^1_{13,23}x_{8,2} + k^1_{13,24}x_{8,3} = f^1_{5,1} \\ k^1_{14,1}x_{1,1} + k^1_{14,2}x_{1,2} + \cdots + k^1_{14,23}x_{8,2} + k^1_{14,24}x_{8,3} = f^1_{5,2} \\ k^1_{15,1}x_{1,1} + k^1_{15,2}x_{1,2} + \cdots + k^1_{15,23}x_{8,2} + k^1_{15,24}x_{8,3} = f^1_{5,3} \end{cases} \tag{13}$$

In the dynamic equations of element 3, the equations which are relevant to the force acting on node 5 can be written as

$$\begin{cases} k^3_{13,1}x_{1,1} + k^3_{13,2}x_{1,2} + \cdots + k^3_{13,23}x_{8,2} + k^3_{13,24}x_{8,3} = f^3_{5,1} \\ k^3_{14,1}x_{1,1} + k^3_{14,2}x_{1,2} + \cdots + k^3_{14,23}x_{8,2} + k^3_{14,24}x_{8,3} = f^3_{5,2} \\ k^3_{15,1}x_{1,1} + k^3_{15,2}x_{1,2} + \cdots + k^3_{15,23}x_{8,2} + k^3_{15,24}x_{8,3} = f^3_{5,3} \end{cases} \tag{14}$$

The resultant force acting on the internal node in a FE model is zero, while the surface node is the external force. The force vectors on the right part of Eqs. (13) and (14) are $(f^1_{5,1}, f^1_{5,2}, f^1_{5,3})$ and $(f^3_{5,1}, f^3_{5,2}, f^3_{5,3})$, respectively. In the model shown in Fig. 6b, the 5th node is an internal node, the resultant force of which is zero. Thus, we can assemble Eqs. (13) and (14) to obtain Eq. (15).

$$\begin{aligned} &k^1_{13,1}x_{1,1} + \cdots + k^1_{13,12}x_{4,3} + \left(k^1_{13,13} + k^3_{1,1}\right)x_{5,1} + \cdots \\ &+\left(k^1_{13,24} + k^3_{1,12}\right)x_{8,3} + k^3_{1,13}x_{9,1} + \cdots + k^3_{1,24}x_{12,3} = f^1_{5,1} + f^3_{5,1} \end{aligned} \tag{15a}$$

$$\begin{aligned} &k^1_{14,1}x_{1,1} + \cdots + k^1_{14,12}x_{4,3} + \left(k^1_{14,13} + k^3_{2,1}\right)x_{5,1} + \cdots \\ &+\left(k^1_{14,24} + k^3_{2,12}\right)x_{8,3} + k^3_{2,13}x_{9,1} + \cdots + k^3_{2,24}x_{12,3} = f^1_{5,2} + f^3_{5,2} \end{aligned} \tag{15b}$$

$$\begin{aligned} &k^1_{15,1}x_{1,1} + \cdots + k^1_{15,12}x_{4,3} + \left(k^1_{15,13} + k^3_{3,1}\right)x_{5,1} + \cdots \\ &+\left(k^1_{15,24} + k^3_{3,12}\right)x_{8,3} + k^3_{3,13}x_{9,1} + \cdots + k^3_{3,24}x_{12,3} = f^1_{5,3} + f^3_{5,3} \end{aligned} \tag{15c}$$

The force balance equations relevant to the other connected nodes can be obtained in the same way. Thus, the dynamic equation of one connection can be written as

$$\begin{bmatrix} \mathbf{K}^1_a & \mathbf{K}^1_b & & \\ \mathbf{K}^1_c & \mathbf{K}^1_d + \mathbf{K}^3_a & \mathbf{K}^3_b & \\ & \mathbf{K}^3_c & \mathbf{K}^3_d + \mathbf{K}^2_a & \mathbf{K}^2_b \\ & & \mathbf{K}^2_c & \mathbf{K}^2_d \end{bmatrix} \{\mathbf{X}\} = \{\mathbf{F}\} \tag{16}$$

where

$$\{\mathbf{X}\} = \left(x_{1,1}, x_{1,2}, x_{1,3}, \ldots, x_{16,1}, x_{16,2}, x_{16,3}\right) \quad \text{and}$$

$$\begin{aligned} \{\mathbf{F}\} = \Big(&f^1_{1,1}, f^1_{1,2}, f^1_{1,3}, \cdots, f^1_{4,1}, f^1_{4,2}, f^1_{4,3} \\ &f^1_{5,1} + f^3_{5,1}, f^1_{5,2} + f^3_{5,2}, f^1_{5,3} + f^3_{5,3}, \cdots, f^1_{8,1} + f^3_{8,1}, f^1_{8,2} + f^3_{8,2}, f^1_{8,3} \\ &+f^3_{8,3}, f^3_{9,1} + f^2_{9,1}, f^3_{9,2} + f^2_{9,2}, f^3_{9,3} + f^2_{9,3} \cdots, f^3_{12,1} + f^2_{12,1}, f^3_{12,2} \\ &+f^2_{12,2}, f^3_{12,3} + f^2_{12,3}, \quad f^2_{13,1}, f^2_{13,2}, f^2_{13,3}, \cdots, f^2_{16,1}, f^2_{16,2}, f^2_{16,3}\Big) \end{aligned}$$

In the same way, connection by connection, the dynamic equations of all the connections can be established.

4 Modeling method application

To show the behavior of the modeling method proposed in this study, two examples are presented. In the first example, the dynamic model of a seven-five axis machine tool is shown. In the second, the dynamic model of an assembly of the bed and base in a gear hobbing machine is shown. In the two examples, the simulated results obtained from the FE dynamic model are compared with the experimental results.

4.1 The frame of the seven-five axis machine tool

4.1.1 Experimental modal analysis

For the frame of the seven-five axis machine tool, the beam is connected to each column by 16 M36 bolts, and the distribution of bolts is shown in Fig. 6. An impact modal testing is

Table 6 Experimental and FEM simulation modal shapes

1	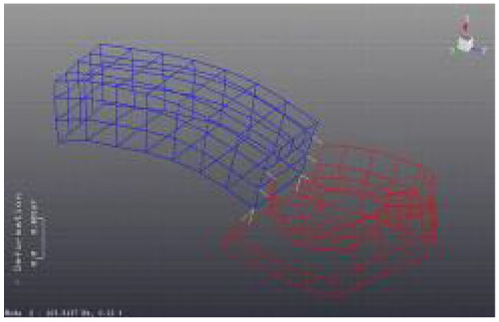	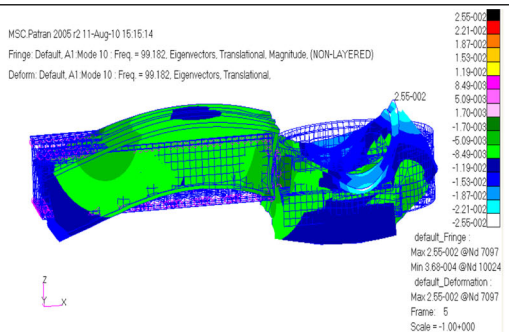	0.956
2	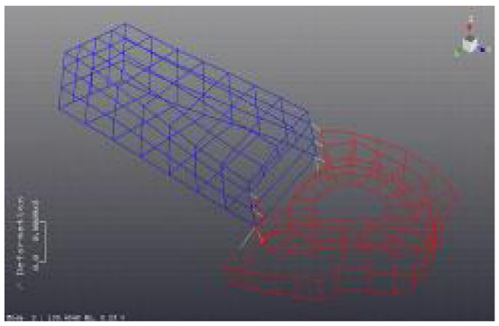	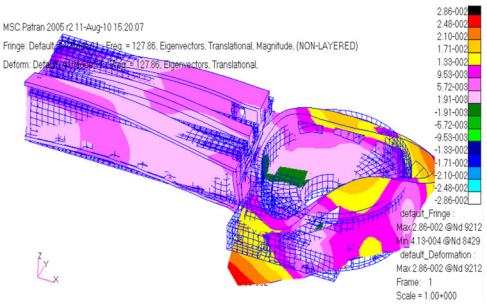	0.965
3	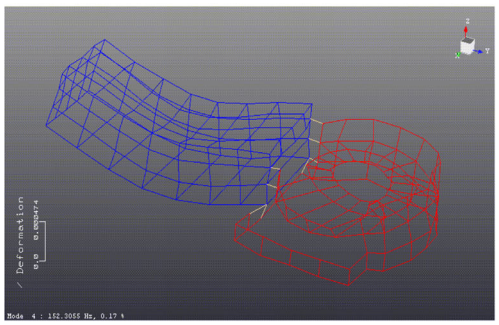	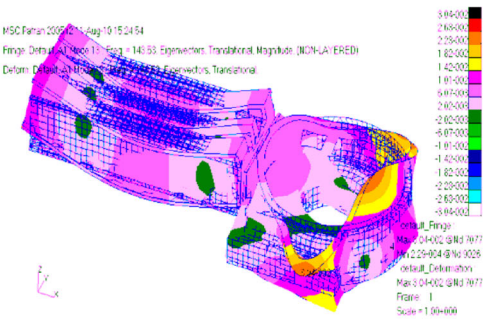	0.968
4	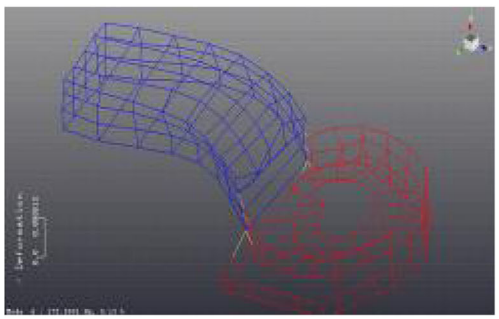	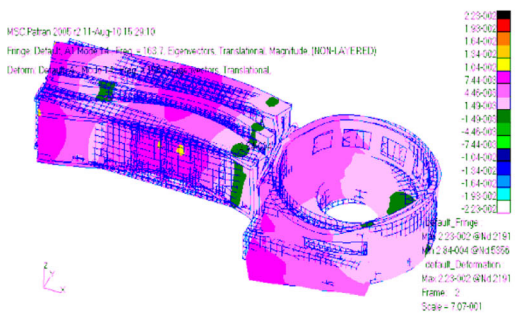	0.972
5	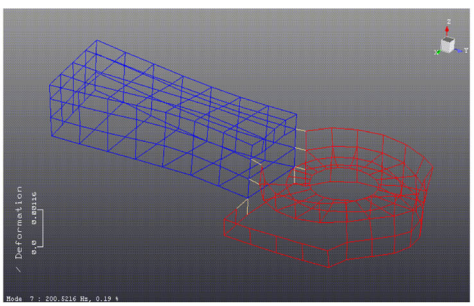	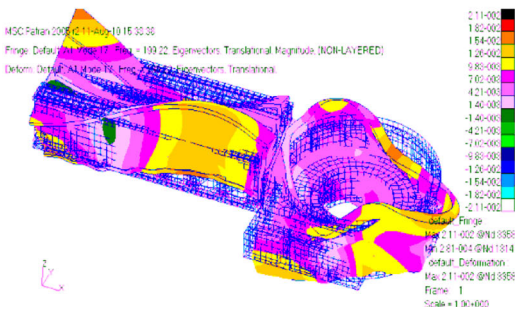	0.943

Table 7 Comparison of modal results

Modal shape	Experimental result (Hz)	FE result (Hz)	Errors (%)
X-axis first-order bending	103.9	99.2	4.5
Y-axis first-order reversing	130.5	127.9	2
Bed *X*-axis first-order bending, base *Y*-axis first-order bending	152.3	143.5	5.7
Z-axis first-order bending	172.6	163.7	5.2
Y-axis second-order reversing	200.5	199.2	0.7

executed on the machine tool. As shown in Fig. 8, the experimental system is described as follows:

(i) The two columns of the machine tools are fixed to the ground. The pretightened torque of the bolts that connect the beam to the columns is 500 Nm. The roughness of the contact surfaces is $R_a = 3.2$ μm.
(ii) The driving point and response points are shown in Fig. 8b. There are 396 response points in total. The LMS SCADAS mobile acquisition is used as the testing system. An impact hammer (made in Beijing Vibration and Noise Institute) is used to excite the machine tools at the fixed driving point in the *Z*-direction. The responses are measured by several low mass, wide bandwidth, three-axis accelerometers (PCB356A16) at all response points. To obtain a column of the FRF matrix, the point FRF at the driving point also needs to be tested.
(iii) The acquisition bandwidth and frequency resolution are 256 and 0.5 Hz, respectively. To reduce the effects of measurement noise and random errors, the force and acceleration signals are obtained by repeated acquisition, and the average values are therefore calculated to estimate the FRFs.

The modal parameters of the machine tools are obtained by using the modal analysis module of the LMS Test.lab. The TDOF method is chosen due to the small damping. The first five-order modal results (modal frequencies and mode shapes) are shown in Table 4.

4.1.2 Numerical model using the proposed method

The numerical model of the machine tools is established using the FEM according to the hybrid analytic-experimental modeling method proposed in this study. The FE model is shown in Fig. 9. The beam and columns (structural components) are modeled by 19,856 hexahedral elements and 658 pentahedral elements in the FE software-MSC.patran, and the material parameters of the components are shown in Table 3. The bolted joint (machine elements) between the beam and columns is modeled by the bolted joint elements. According to the dynamic modeling of the bolted joint mentioned in Section 2.2, each of the bolted joint interfaces is divided into 16 bolted joint elements. The stiffness matrices of the bolted joint elements are obtained from the bolted joint element stiffness matrix database according to the size, roughness of the contact surface, and the pretightened force of the bolts of every bolted joint, and the stiffness matrices are inserted into the finite element model through direct matrix input at the grid points (DMIG) in MSC.patran.

Executing a normal model analysis, the modal results of the machine tools, such as the natural frequencies and corresponding mode shapes, are obtained. Comparisons between the FE simulation results and the experimental modal results are shown in Tables 4 and 5. Except for the first-order mode shape, the errors found in the natural frequencies between FE simulation results and the experimental modal results are less than 6 %, which indicates that the proposed hybrid method in this study is effective. It should be mentioned that the boundary condition of the columns is treated as fixed condition in the numerical model, which is the main factor that leads to the higher error of the first-order mode.

4.2 The assembly of the bed and base of the gear hobbing machine

4.2.1 Experimental modal analysis

The second example consists of an assembly of the bed and base in a moving column gear hobbing machine. The assembly is an important structural component, which acts as the mounting base for the rolling guides and working table. The bed and the base are connected by eight M36 bolts. The experimental system is similar to that shown in Fig. 8; the differences from the above shown experiment are the following:

(i) The assembly is placed on several wooden blocks to simulate the free-to-free boundary conditions. The pretightened torque of the connected bolts is 500 Nm. The roughness of the contact surfaces is $R_a = 3.2$ μm.
(ii) The LMS SCADAS mobile acquisition is used as the testing system. The driving point and response points are shown in Fig. 10, and there are 212 response points in total. The impact hammer excites the assembly at the fixed driving point in the *Z*-direction. Twenty-three axis accelerometers are used to acquire the FRF data. The SIMO method is performed in the experiment to obtain all the FRFs.
(iii) The acquisition bandwidth and frequency resolution are 520 and 0.5 Hz, respectively.

The modal parameters of the assembly are obtained using the LMS Test.lab vibration analysis system. The first five-order modal results (modal frequencies and mode shapes) are shown in Table 5.

4.2.2 Numerical model using the proposed method

The FE model of the assembly is shown in Fig. 11. The bed and base (structural components) are modeled by 28,233 hexahedral elements and 3176 pentahedral elements in the FE software-MSC.patran, and the material parameters of the components are shown in Table 3. The bolted joint (machine elements) between the bed and base is modeled by nine bolted joint elements. The stiffness matrices of the bolted joint elements are obtained using the same method as in Section 4.1 and are inserted into the finite element model through DMIG in MSC.patran.

Executing normal model analysis, the modal results of the assembly, such as the natural frequencies and corresponding mode shapes, are obtained. Comparisons between the FE simulation results and the experimental modal results are shown in Tables 6 and 7. It is easy to see that the errors between FE simulation results and the experimental modal results of the natural frequencies are less than 6 %, which indicates that the proposed hybrid method in this study is effective.

5 Conclusion

Structural dynamics notably affect the performance of machine tools. Due to the many complex joints, establishing a full machine tool dynamic model is a difficult task. In this paper, a hybrid analytic-experimental dynamic modeling method for modeling of the entire machine tool structure is proposed. The whole machine tool is assembled by the numerical model of structural components and the experimental model of machine elements. The bolted joint is taken as an example for illustrating the dynamic modeling of machine elements. Two cases are presented to illustrate the behavior of the proposed modeling method. The comparison between experimental natural frequencies and the simulated ones in the two presented cases indicates that the proposed hybrid analytic-experimental dynamic modeling method is effective.

Like machine tool structure modeling, the method proposed in this paper can be used for the modeling of other mechanical systems, such as a diesel engine and gear reducer. For example, the dynamic model of the gear reducer box, which is composed of an upper box and lower box, can be obtained using the proposed modeling method. The upper and lower boxes can be modeled using the FEM, and the joint between the two boxes can be modeled using the bolted joint element presented in this paper; therefore, the full dynamic model can be obtained by assembling the two dynamic models. Thus, the method provides a possible way for the full structural dynamic model of mechanical systems such as machine tools. However, except for the bolted joint, the universal dynamic model of other joints will be discussed in the future because of their complexity.

Acknowledgments This work was supported by the National Science and Technology Support Program of China, Grant No. 2012BAF08B01, and the National Basic Research Program of China, Grant No. 2005CB724101. The authors are grateful to other participants of the projects.

References

1. Altintas Y, Brecher C, Weck M, Witt S (2005) Virtual machine tool. CIRP Ann Manuf Technol 54(2):115–138
2. Vesely J, Sulitka M (2008) Machine tool virtual model. In International Congress Matar Praha, 115–122
3. Brecher C, Esser M, Witt S (2009) Interaction of manufacturing process and machine tool. CIRP Ann Manuf Technol 58(2):588–607
4. Brecher C, Witt S (2009) Interactive analysis of the structural mechanic behaviour of machine tools. Prod Eng 3(4-5):475–481
5. Lee RS, Lin YH (2010) Development of universal environment for constructing 5-axis virtual machine tool based on modified D–H notation and OpenGL. Robot Comput Integr Manuf 26(3):253–262
6. Kadir AA, Xu X, Hämmerle E (2011) Virtual machine tools and virtual machining—a technological review. Robot Comput Integr Manuf 27(3):494–508
7. Ding WZ, Huang XD, Wang ML, Zhu SQ (2013) An approach to evaluate the effects of nonlinear traveling joints on dynamic behavior of large machine tools. Int J Adv Manuf Technol 68(9):2025–2032
8. Zatarain M, Lejardi E, Egana F, Bueno R (1998) Modular synthesis of machine tools. CIRP Ann Manuf Technol 47(1): 333–336
9. Tlusty J, Ziegert JC, Ridgeway S (2000) A comparison of stiffness characteristics of serial and parallel machine tools. J Manuf Process 2(1):67–76
10. Huang DT-Y, Lee J-J (2001) On obtaining machine tool stiffness by CAE techniques. Int J Mach Tools Manuf 41(8):1149–1163
11. Doman D, Warkentin A, Bauer R (2009) Finite element modeling approaches in grinding. Int J Mach Tools Manuf 49(2):109–116
12. Bais R, Gupta A, Nakra B, Kundra T (2004) Studies in dynamic design of drilling machine using updated finite element models. Mech Mach Theory 39(12):1307–1320
13. Ford DG, Widiyarto MHN, Myers A, Longstaff AP, Fletcher S (2014) Structural analysis and characterisation technique applied to a CNC vertical machining centre. Proc Inst Mech Eng C J Mech Eng Sci 228(13):2357–2371
14. Liang Y, Chen W, Bai Q, Sun Y, Chen G, Zhang Q, Sun Y (2013) Design and dynamic optimization of an ultraprecision diamond flycutting machine tool for large KDP crystal machining. Int J Adv Manuf Technol 69(1):237–244
15. Huo D, Cheng K, Wardle F (2010) Design of a five-axis ultra-precision micro-milling machine—UltraMill. Part 2: integrated dynamic modelling, design optimisation and analysis. Int J Adv Manuf Technol 47(9):879–890
16. Aurich JC, Biermann D, Blum H, Brecher C, Carstensen C, Denkena B, Klocke F, Kröger M, Steinmann P, Weinert K (2009) Modelling and simulation of process: machine interaction in grinding. Prod Eng 3(1):111–120

17. Fleischer J, Munzinger C, Tröndle M (2008) Simulation and optimization of complete mechanical behaviour of machine tools. Prod Eng 2(1):85–90
18. Brecher C, Witt S (2006) Simulation of machine process interaction with flexible multi-body simulation. In Proceedings of the 9th CIRP international workshop on modeling of machining operations, Bled, Slovenia, 171–178
19. Cano T, Chapelle F, Lavest J-M, Ray P (2008) A new approach to identifying the elastic behaviour of a manufacturing machine. Int J Mach Tools Manuf 48(14):1569–1577
20. Zhang G, Huang Y, Shi W, Fu W (2003) Predicting dynamic behaviours of a whole machine tool structure based on computer-aided engineering. Int J Mach Tools Manuf 43(7):699–706
21. Renton D, Elbestawi M (2001) Motion control for linear motor feed drives in advanced machine tools. Int J Mach Tools Manuf 41(4): 479–507
22. Zaeh M, Siedl D (2007) A new method for simulation of machining performance by integrating finite element and multi-body simulation for machine tools. CIRP Ann Manuf Technol 56(1):383–386
23. Taylor S, Tobias S (1964) Lumped-constants method for the prediction of the vibration characteristics of machine tool structures. In Proc 5th Int MTDR Conf
24. Hijink J, Van Der Wolf A (1974) Analysis of a milling machine: computed results versus experimental data. In Proceedings of the fourteenth international machine tool design and research conference 553–558
25. Beards C (1982) Damping in structural joints. Shock Vib Inf Center Shock Vib Dig 14(6):9–11
26. Tlusty J, Ismail F (1980) Dynamic structural identification tasks and methods. CIRP Ann Manuf Technol 29(1):251–255
27. Ahmadian H, Jalali H (2007) Identification of bolted lap joints parameters in assembled structures. Mech Syst Signal Process 21(2):1041–1050
28. Tian H, Li B, Liu H, Mao K, Peng F, Huang X (2011) A new method of virtual material hypothesis-based dynamic modeling on fixed joint interface in machine tools. Int J Mach Tools Manuf 51(3):239–249
29. Mao K, Li B, Wu J, Shao X (2010) Stiffness influential factors-based dynamic modeling and its parameter identification method of fixed joints in machine tools. Int J Mach Tools Manuf 50(2):156–164
30. Shamine DM, Shin YC (2000) Analysis of no. 50 taper joint stiffness under axial and radial loading. J Manuf Process 2(3):167–173
31. Namazi M, Altintas Y, Abe T, Rajapakse N (2007) Modeling and identification of tool holder–spindle interface dynamics. Int J Mach Tools Manuf 47(9):1333–1341
32. Xu C, Zhang J, Wu Z, Yu D, Feng P (2013) Dynamic modeling and parameters identification of a spindle–holder taper joint. Int J Adv Manuf Technol 67(5–8):1517–1525
33. Kolar P, Sulitka M, Janota M (2011) Simulation of dynamic properties of a spindle and tool system coupled with a machine tool frame. Int J Adv Manuf Technol 54(1):11–20
34. Okwudire CE, Altintas Y (2009) Hybrid modeling of ball screw drives with coupled axial, torsional, and lateral dynamics. J Mech Des 131(7):071002
35. Vicente DA, Hecker RL, Villegas FJ, Flores GM (2012) Modeling and vibration mode analysis of a ball screw drive. Int J Adv Manuf Technol 58(1–4):257–265
36. Dhupia JS, Ulsoy AG, Katz R, Powalka B (2008) Experimental identification of the nonlinear parameters of an industrial translational guide for machine performance evaluation. J Vib Control 14(5):645–668
37. Ohta H, Tanaka K (2010) Vertical stiffnesses of preloaded linear guideway type ball bearings incorporating the flexibility of the carriage and rail. J Tribol 132(1):011102
38. Shaw D, Su W (2013) Stiffness analysis of linear guideways without preload. J Mech 29(02):281–286
39. Li H, Li B, Mao K, Huang X, Peng F (2014) A parameterized model of bolted joints in machine tools. Int J Acoust Vib 19(1):10–20